

A new approach to the continuum modeling of epitaxial growth: slope selection, coarsening, and the role of the uphill current

Tak Shing Lo and Robert V. Kohn

kohn@cims.nyu.edu and *tslo@cims.nyu.edu*

Courant Institute of Mathematical Sciences

New York University

New York, NY 10012

Revised version: October 1, 2001

Abstract

We develop a new approach to the macroscopic modeling of epitaxial growth, focusing on the slope-selection and coarsening observed in spiral-mode growth. Our model distinguishes between the surface height and the surface adatom density. These quantities evolve by a coupled pair of partial differential equations: a Hamilton-Jacobi equation for the height, coupled to a nonlinear diffusion equation for the adatom density. The influence of the Ehrlich-Schwoebel barrier is included through an “uphill current” in the equation for adatom density. Our model predicts slope selection and coarsening – thus it offers a possible mechanism for these effects. The model predicts, in particular, that the coarsening rate depends mainly on the strength of the Ehrlich-Schwoebel barrier.

PACS numbers: 68.55-a (Thin film structure and morphology); 81.15.Aa (Theory and models of film growth).

keywords: epitaxial growth, slope selection, Ehrlich-Schwoebel barrier.

1 Introduction

Epitaxial growth is a complex, multiscale, far-from-equilibrium process [1, 2, 3, 4]. There are many regimes, associated with different microscopic mechanisms and leading to different types of spatial structure. This paper addresses a particular regime, spiral growth, whose mesoscopic behavior includes slope-selection and coarsening. We shall elucidate these phenomena by developing and applying a new type of continuum growth model.

Our attention is on mesoscopic features – spatial structure whose length scale is large compared to the lattice size but small compared to the sample size. It is therefore natural to seek a continuum-type model, i.e. one expressed by a partial differential equation (PDE).

Much of the recent work on continuum growth models has addressed kinetic roughening during molecular beam epitaxy (MBE). The film height is typically modeled by a nonlinear PDE like

$$h_t = c_1 \Delta h + c_2 |\nabla h|^2 + c_3 \Delta^2 h + c_4 \Delta(|\nabla h|^2) + \text{deposition flux} + \text{noise}. \quad (1)$$

Such models have been shown to capture many aspects of kinetic roughening, and to be consistent with Monte Carlo models, see e.g. [5, 6, 7, 8, 9, 10, 11, 12, 13, 14].

The present article addresses a different growth regime: the late-stage coarsening of grains formed by spiral growth. In this context, height is gained not by nucleation of islands, but rather by the action of screw dislocations. Roughness is due not to atomic-scale stochasticity, but rather to the grain structure induced by spiral growth. Our model is therefore quite different from (1). Briefly, it specifies the surface height h and the surface adatom density ρ by a coupled system of PDE's:

$$\nu h_t = \alpha \rho |\nabla h| + \frac{\beta}{(A + |\nabla h|)} \rho^2 \quad (2)$$

$$\rho_t = D \Delta \rho - S \nabla \cdot (\rho \nabla h) - \alpha \rho |\nabla h| - \frac{\beta}{(A + |\nabla h|)} \rho^2 - \frac{\rho}{\tau} + F \quad (3)$$

The physical origin of these equations will be explained presently.

The microscopic mechanisms of spiral growth have been explored at length, see e.g. [1, 2, 3, 15, 16, 17], but we know only a little work attempting to model such growth at the continuum scale [18, 19, 20]. The high temperature superconductor $\text{YBa}_2\text{Cu}_3\text{O}_7$ provides a

convenient experimental system [21, 22] for investigating this type of growth. Good quality films of c-axis YBCO are in demand for microelectronic applications. Such films can be grown by a variety of deposition methods, on a variety of different substrates. The surface of the film has a distinctive structure of peaks and valleys. The peaks are associated with the screw dislocations, while the valleys mark the grain boundaries. The peaks are more or less conical and the valleys have sharp edges. As growth proceeds, *coarsening* and *slope selection* are observed – in other words, the density of peaks at the film surface decreases and the grain size increases, while the slope of the grains on the surface remains fairly uniform. These trends have been seen in several studies [21, 22, 23, 24], though the data are too sparse to support firm quantitative conclusions about the coarsening rate.

We shall show that the model specified by (2) and (3) captures, in a phenomenological but natural way, the essential physics of this system. Our approach is admittedly unconventional: the film height does not solve a scalar PDE similar to (1). Rather, we use a *coupled system* of differential equations for the film height $h(x, t)$ and the surface adatom density $\rho(x, t)$. The equations given above are the ones that we actually compute – with specific values of the constants ν , α , β , A , D , S , and τ , chosen to give qualitative agreement with the behavior of YBCO. Equations (2)-(3) arise by specialization from the more general model

$$\nu h_t = \phi_{\text{attach}} |\nabla h| + \psi_{\text{nucl}} \tag{4}$$

$$\rho_t = D\Delta\rho - K\nabla \cdot (\phi_{\text{attach}} \nabla h) - \phi_{\text{attach}} |\nabla h| - \psi_{\text{nucl}} - (\rho/\tau) + F . \tag{5}$$

The meaning of each term is explained in detail in Section 2. But briefly: the equation for h_t expresses how growth results from attachment at steps (modeled through ϕ_{attach}) and nucleation of new height through the action of screw dislocations (modeled through ψ_{nucl}). The equation for ρ_t expresses how the density of adatoms on the surface changes due to diffusion, attachment, nucleation, evaporation, and deposition. The factor ν in front of h_t is the number of cells of the growing lattice per unit volume; notice that if evaporation is negligible ($\tau = \infty$) then mass is conserved:

$$\frac{d}{dt} \int (\nu h + \rho) dx = \int F dx \tag{6}$$

provided the boundary conditions for ρ permit the associated integration by parts.

While we focus on spiral growth, the coarsening of fully-developed mounds in molecular beam epitaxy can be described similarly. The main difference is that in mounding, new height is gained by nucleation of islands at the peaks rather than by the action of screw dislocations.

Use of a coupled system to model epitaxial growth is unconventional – but it seems to us quite natural. In distinguishing between the film height and the surface adatom density, we recognize that adatoms are the actual objects which diffuse on the surface. This approach originates in recent work by E, Schulze and Yip [25, 26], where equations similar to (4)–(5) have been derived by coarse-graining specific microscopic growth models.

An important atomic-scale effect is the Ehrlich-Schwoebel barrier, see e.g. [27], [28], and page 94 of [4]. As many authors have recognized – and as we shall explain in Section 2 – the resulting asymmetric attachment law induces an *uphill current*. The term $K\nabla \cdot (\phi_{\text{attach}} \nabla h)$ in our ρ -equation is a phenomenological term representing this uphill current. It may seem strange that the form of the uphill current term is determined by ϕ_{attach} ; we shall explain this in Section 2.

After specifying and calibrating our model, we shall show by direct two-dimensional numerical simulation that it predicts both slope selection and coarsening. Interestingly, the coarsening rate depends mainly on the strength of the Ehrlich-Schwoebel barrier. We shall explain the origin of this trend – and, more generally, the qualitative sources of slope selection and coarsening – by examining the one-dimensional version of our model. In particular, we shall show that the prediction of slope selection and coarsening is robust: these qualitative effects arise from the basic structure of the model, not from the details of our constitutive laws.

Besides explaining slope-selection and coarsening, our approach has two important conceptual advantages over more standard continuum growth models. First: it clarifies the role of the uphill current associated with the Ehrlich-Schwoebel barrier, by representing it as a single term $K\nabla \cdot (\phi_{\text{attach}} \nabla h)$ in the adatom diffusion equation. Second: our approach generalizes naturally to a multispecies setting, by replacing the adatom diffusion equation (5) with separate equations for each species. Such a multispecies model should be useful for analyzing the growth of a compound solid thin film such as YBCO, where stoichiometry

is critical. The calibration of a multispecies model is difficult, however, for lack of data; therefore we restrict our attention in this paper to the single-species setting.

Our treatment of “nucleation” has no correspondence in the recent work of E, Schulze, and Yip [25, 26]. Those authors addressed coarse-graining of growth on a length scale much larger than the terrace width but smaller than the grain size. Therefore, their attention was on the region far from any peak or valley, where the atomic-scale configuration resembles a steady step train; little attention was devoted to the behavior at peaks, where new height is gained. Our interest is different: we wish to study growth on a length scale of many grains. For this purpose, the modeling of “nucleation” – more precisely, creation of new height at peaks – is crucial. We shall explain in Section 2 why our choice of the term ψ_{nucl} accounts for nucleation in a phenomenological but reasonable way.

We also depart from the work of E, Schulze, and Yip by including the effect of evaporation. For most methods of deposition, evaporation of adatoms is believed to be relatively insignificant. It is however easy to include in the model, and it may be important in some settings – for example, in chemical vapor deposition where evaporation provides a natural source of feedback from the growing film to the reactor environment [29].

There is another body of work that distinguishes between height and surface composition – namely the recent literature on surface instabilities of growing alloys, see e.g. [30, 31, 32]. These authors’ goals and methods are however very different from ours. They focus on the instability of a flat surface due to the combined effects of elastic misfit, surface diffusion, and phase separation. We focus, by contrast, on coarsening rather than instability. Moreover, our attention is on the kinetics of attachment at steps and nucleation at peaks, ignoring the effects of stress, curvature, and phase separation. Yet another approach to multicomponent growth can be found in [33].

The rest of this article is organized as follows. Section 2 discusses the physical meaning of our coupled-system growth model. Section 3 provides additional details about the system that we actually compute, (2)-(3). Section 4 reports the predictions of the model based on direct numerical simulation. Section 5 discusses the essential mechanisms of slope selection and coarsening. Section 6 summarizes our accomplishments and compares our work to other treatments of slope selection and coarsening based on equations similar to (1).

2 The model

This section explains the physical meaning of our coupled system (4)–(5), and our choice of constitutive laws for the “attachment” and “nucleation” terms.

2.1 The height equation

Our model addresses growth below the roughening temperature, in a regime where the film surface is atomically stepped (Fig. 1). Adatoms arrive at the terraces (deposition), move around on the terraces (diffusion), and possibly leave the terraces (evaporation), but they get incorporated into the growing crystal (attachment) only at steps. The attachment of adatoms makes the steps advance, sweeping across the terraces.

We think of the film height $h(x, t)$ as a smooth function interpolating between the step heights (Fig. 2). Thus the locus of a step is a level set of h , just as the lines on a topographical survey map are level sets of altitude. A moment’s thought reveals that the horizontal speed of a level set of h is just $h_t/|\nabla h|$.¹ (This relation lies at the heart of the “level-set method” for simulating interface motion, see e.g. [34, 35, 36].)

The physical meaning of the “attachment” term ϕ_{attach} is now clear: it controls the horizontal velocity of the steps. Indeed, if we ignore for a moment the “nucleation” term ψ_{nucl} , then the h -equation becomes

$$\nu h_t = \phi_{\text{attach}} |\nabla h|, \quad (7)$$

which specifies $\nu^{-1}\phi_{\text{attach}}$ as the step velocity.

We need a constitutive law for ϕ_{attach} . Of course it should depend on the adatom density ρ , since attachment of adatoms is what drives the growth. It might also plausibly depend on the width of the terraces and the in-plane curvature of the steps; this would make ϕ_{attach} a function of ρ , $|\nabla h|$ and $\nabla \cdot (\nabla h/|\nabla h|)$. For simplicity, however, we shall use the simplest reasonable constitutive law:

$$\phi_{\text{attach}} = \alpha \rho \quad (8)$$

¹The justification is especially simple when space is one dimensional and steps are points: if $x(t)$ is the position of a step then $h(x(t), t)$ is constant, so $h_x x_t + h_t = 0$, whence $|x_t| = |h_t|/|h_x|$. When space is two dimensional the argument is similar, since the normal velocity of the step is $|x_t \cdot \nabla h|/|\nabla h|$.

where α is a suitable constant.²

The first-order equation (7) is known as a *Hamilton-Jacobi* equation [37]. In regions where h is smooth it can be solved by the method of characteristics. When $\phi = \alpha\rho$ its solution can be represented using a version of Huyghen’s principle, see e.g. [20, 38]. The “wavefronts” are the level sets of h (the loci of steps), while the “rays” are the characteristics of the partial differential equation (curves normal to the steps).

Our derivation of (7) breaks down at peaks and valleys, where the surface is not approximated by a steady step train. This is not a mere technicality: proper modeling of peaks and valleys is crucial. Physically: peaks and valleys are special, because new steps are created at peaks and existing steps are annihilated at valleys. Mathematically: peaks are sources of new characteristics, while valleys are caustics where characteristics collide. (Notice that peaks and valleys can be sharp, i.e. ∇h can be discontinuous, since (7) is a first-order equation.)

How should we model the peaks and valleys? One idea would be to treat them as boundaries, using the atomic-scale physics to determine the appropriate boundary conditions for (7). But the proper form of the boundary condition is unclear. Moreover, simulation of such a law would be cumbersome, since the peaks and valleys would be free boundaries. So it is natural to seek a different, more computable approach.

An important hint is provided by the theory of *viscosity solutions* of Hamilton-Jacobi equations, see e.g. [20, 35, 37]. Such solutions are readily computable, despite the presence of caustics. The definition of a viscosity solution places special conditions on the behavior of h near singularities. For the present purposes, the main point is this: in a viscosity solution all singularities are sinks – not sources – of characteristics. Thus the viscosity solution gets the physics right at the valleys, but not at the peaks. In fact, the viscosity solution of (7) describes horizontal growth without nucleation. Each peak of the initial profile would become a plateau under such a law, and the maximum height would never exceed that of the initial data.

The solutions we desire are different: they must gain new height at the peaks. This is

²In truth, attachment is controlled by the microscopic adatom density *at a step*, while ρ represents the microscopic adatom density *averaged over an entire terrace*. In choosing the constitutive law (8), we are effectively using the latter as a proxy for the former.

the role of the “nucleation” term ψ_{nucl} . We choose it so that ψ_{nucl} is positive at the peaks (where $|\nabla h| \approx 0$) but negligibly small away from peaks (where $|\nabla h|$ is larger). Of course ψ_{nucl} must depend on the adatom density ρ , since growth is driven by the availability of adatoms. For simplicity, we use the constitutive law

$$\psi_{\text{nucl}} = \frac{\beta}{A + |\nabla h|} \rho^2 \quad (9)$$

where β and A are suitable constants (with A sufficiently small).

Our choice (9) is admittedly ad-hoc; it would be just as plausible, for example, to assume linear rather than quadratic dependence in ρ . Perhaps one could derive a refined nucleation term by examining the local details of spiral growth, using tools like those employed in [16] or [17]. Changing the form of ψ_{nucl} would certainly change quantities such as the selected slope and the coarsening rate. But we believe – based on numerical experiments and the analysis in Section 5 – that it would not change the qualitative behavior of our model. Therefore we restrict attention in the present work to the simple and easily-calibrated choice (9).

2.2 The density equation

Adatoms arrive at the surface (deposition); they move around on the surface (diffusion); then they leave the surface, either by being incorporated into the growing film (attachment and nucleation) or by returning to the ambient medium (evaporation). The ρ -equation expresses the balance between these processes. It can be written as

$$\begin{aligned} \rho_t &= \text{diffusion} - \text{attachment} - \text{nucleation} - \text{evaporation} + \text{deposition} \\ &= -\nabla \cdot J - \phi_{\text{attach}} - \psi_{\text{nucl}} - \frac{\rho}{\tau} + F \end{aligned}$$

where J is the adatom current; ϕ_{attach} and ψ_{nucl} are the “attachment” and “nucleation” laws discussed above; τ is the evaporation time; and F is the deposition flux. The presence of the attachment and nucleation terms is dictated by mass conservation, c.f. (6). The evaporation and deposition terms are standard. So only the diffusion term requires explanation.

Our constitutive law for the adatom current is

$$J = -D\nabla\rho + K\phi_{\text{attach}}\nabla h \quad (10)$$

where $D > 0$ and $K \geq 0$ are suitable constants. The first term is the standard Fick’s law, describing the tendency of the adatoms to equilibrate by flowing from regions of high density to regions of low density. The second term is the uphill current associated with the presence of an Ehrlich-Schwoebel barrier. It is quite literally an uphill current: if, for example, ρ is largest at the peaks and smallest at the valleys (which, as we shall see, is typical), then $-D\nabla\rho$ points downhill while $K\phi_{\text{attach}}\nabla h$ points uphill, provided D , K and ϕ_{attach} are all positive.

The “Schwoebel” term $K\phi_{\text{attach}}\nabla h$ plays a critical role in our model: without it there is no coarsening. Let us therefore review its microscopic origin. The following discussion summarizes the treatment in [25]; different (but related) discussions can be found in [39, 40, 41]. Consider a uniform one-dimensional step train (Fig. 3). We assume that, at the atomic scale, adatoms are arriving randomly at constant rate F . After arriving, the adatoms diffuse along the surface – possibly crossing from one terrace to the next, and never interacting if they meet. When an adatom is just above or just below a step, there is a certain probability that it attaches at the step; its diffusion terminates when attachment occurs. The attachment rate from the top of a step is typically lower than that from the bottom of a step; this asymmetry is, for our purposes, the main consequence of the Ehrlich-Schwoebel barrier.

Consider now the effect of a large Ehrlich-Schwoebel barrier. It dictates that attachment occurs mainly from below the steps. So most adatoms attach to the film at points uphill from their starting points. Thus the average adatom current – the average over a terrace of the local adatom current – points uphill, even in the absence of a macroscopic gradient of adatom density. The magnitude of this uphill current is proportional to the arrival rate F . At steady-state, ignoring nucleation and evaporation, mass conservation dictates that arrivals and departures occur at the same rate, so $F = \phi_{\text{attach}}|\nabla h|$. Thus the uphill current due to the Schwoebel barrier is proportional to $\phi_{\text{attach}}|\nabla h|$. Since it must point uphill, its form is thus $K\phi_{\text{attach}}\nabla h$ for some choice of the constant K .

2.3 Remarks

The model we actually work with is the coupled system (2)-(3). It is obtained as a special case of the more general model (4)-(5) by choosing ϕ_{attach} and ψ_{nucl} as specified above, then

setting $S = K\alpha$ for simplicity of notation.

The h -equation does not have a second-order (diffusion) term, so its solution can and will have a slope discontinuity at each valley. The numerical solution scheme must be chosen with care so it gives the viscosity solution of this Hamilton-Jacobi equation; we shall return to this point in Section 3.

The ρ -equation has the second-order diffusion term $D\Delta\rho$, so it presents no mathematical difficulties. The uphill current $S\nabla \cdot (\rho\nabla h)$ does not interfere with well-posedness, because it is a first-order term in ρ .

Spiral growth is not symmetric under the inversion $h \rightarrow -h$: the peaks of the surface profile are at points, representing screw dislocations, while the valleys are at curves, representing grain boundaries. Our model captures this asymmetry by using the viscosity solution of (2) – which, by its very definition, treats peaks and valleys differently.

3 Calibration

This section nondimensionalizes our model and gives details of our numerical discretization. Then it explains how the constants α , β , A , D , S , τ and F should be chosen to achieve qualitative agreement with a typical experimental regime.

3.1 Nondimensionalization

Let a be the size of a cell in the growing lattice. Also let v and F_0 be the typical experimental growth rate and deposition flux, respectively. Rescaling lengths by the evaporation length $\sqrt{D\tau}$, time by the monolayer time a/v , F by F_0 and ρ by $F_0\tau$, (2) and (3) can be written in the following dimensionless form:

$$\frac{\partial \tilde{h}}{\partial \tilde{t}} = \tilde{\alpha}_1 \tilde{\rho} |\tilde{\nabla} \tilde{h}| + \frac{\tilde{\beta}_1}{(A + |\tilde{\nabla} \tilde{h}|)} \tilde{\rho}^2, \quad (11)$$

$$\frac{\partial \tilde{\rho}}{\partial \tilde{t}} = \frac{1}{\tilde{\tau}} \tilde{\Delta} \tilde{\rho} - \tilde{S} \tilde{\nabla} \cdot (\tilde{\rho} \tilde{\nabla} \tilde{h}) - \tilde{\alpha}_2 \tilde{\rho} |\tilde{\nabla} \tilde{h}| - \frac{\tilde{\beta}_2}{(A + |\tilde{\nabla} \tilde{h}|)} \tilde{\rho}^2 - \frac{\tilde{\rho}}{\tilde{\tau}} + \frac{\tilde{F}}{\tilde{\tau}}. \quad (12)$$

Here the variables marked by tilde are normalized quantities. The dimensionless parameters are related to the phenomenological parameters through

$$\tilde{\alpha}_1 = \frac{F_0}{\nu} \sqrt{\frac{\tau}{D}} \tilde{\alpha}_2, \quad \tilde{\beta}_1 = \frac{F_0}{\nu} \sqrt{\frac{\tau}{D}} \tilde{\beta}_2,$$

and

$$\tilde{\tau} = \frac{v\tau}{a}, \quad \tilde{S} = \frac{Sa}{v\sqrt{D\tau}}, \quad \tilde{\alpha}_2 = \frac{\alpha a}{v}, \quad \tilde{\beta}_2 = \frac{\beta a F_0 \tau}{v}.$$

From now on, we shall drop the tildes in the dependent and independent variables, and all quantities are normalized unless otherwise stated.

3.2 Method of computation

To solve (11) and (12), we first use the product rule to rewrite the uphill current term in the form

$$(\rho \Delta h + \nabla \rho \cdot \nabla h). \quad (13)$$

Then the gradients and Laplacians, except the terms $|\nabla h|$, are approximated by using centered differences. It is well-known that approximating the term $|\nabla h|$ in a Hamilton-Jacobi equation by ordinary centered differencing will result in undesirable numerical instabilities in the solutions [35], so special treatment must be given to such terms. In our computations, we use an upwind differencing scheme suggested in [35] to obtain the *viscosity solution* of the Hamilton-Jacobi equation. In the one-dimensional version, this scheme is equivalent to the usual upwind differencing scheme for a hyperbolic PDE, except at the peak and the valley where the slopes are ambiguous. At a peak, the scheme is designed to treat it as a point with zero slope; at a valley, it assigns $|h_x|$ a value equal to its left hand or right hand limit, whichever is greater in magnitude. Thus the peaks are infinitesimally smooth ($|h_x| = 0$ at one grid point) while the valleys are infinitesimally sharp ($|h_x|$ jumps discontinuously). This is the type of behavior one expects at the peaks and valleys of a growing thin film. Finally, (11) is stepped forward in time by using the explicit Euler scheme. In the one-dimensional case, we step (12) forward in time by treating the diffusion term implicitly and all the other terms explicitly. In our two-dimensional simulations, it is stepped forward in time by applying the ADI (alternating direction implicit) scheme to the diffusion term, see e.g. [42].

3.3 Choices of parameters

Rather than simply give values for the parameters, we shall explain how we arrive at the values we use. The argument reveals the effect of varying each parameter, and also shows a lot of important information about our model.

The overall idea, of course, is to make the typical features of the solutions match those of the experimental data. In practice, we assess the “typical features” of the solutions by examining the growth of a *periodic array of grains*. This could be done in two space dimensions, but the one-dimensional version is more transparent and quite sufficient. So we shall focus in this subsection on the one-dimensional analogue of (2)-(3), with periodic boundary conditions.

The relevant experimental observations are the growth rate, slope, and grain size. For c-axis YBCO films made by off-axis RF magnetron sputtering, Raistrick and Hawley report a growth rate of $.06 - .09 \mu\text{m/hr}$, with grain sizes around $325 - 500 \text{ nm}$ when the film thickness is 500 nm (about 425 monolayers) [21]. Their STM images indicate a slope around $.02 - .04$. Other deposition mechanisms for c-axis YBCO produce similar morphologies, but the growth rate varies considerably; for example, [24] reports growth at about $5 \mu\text{m/hr}$ using pulsed laser decomposition. Our goal was a qualitative match to a typical growth regime, not a quantitative match to a specific data set. Therefore for calibration purposes we took the growth rate to be about $1 \mu\text{m/hr}$ and the slope to be about $.01$.

Let’s begin by looking for a steadily-growing profile with constant vertical velocity v , constant adatom density ρ and constant adatom current J . The height equation (2) becomes

$$\alpha\rho|h_x| + \frac{\beta}{(A + |h_x|)}\rho^2 = \nu v \quad (14)$$

and the density equation (3) simplifies to

$$\rho = F\tau \left(1 - \frac{\nu v}{F}\right) . \quad (15)$$

Let c be the horizontal velocity of the film, which we can write as $|h_x| = v/c$. Substituting (15) into (14), we can obtain

$$c = \frac{F\tau}{\nu} \left(1 - \frac{\nu v}{F}\right) \left[\alpha + \frac{\beta F\tau}{(v/c)(A + v/c)} \left(1 - \frac{\nu v}{F}\right) \right] . \quad (16)$$

As noted above, typical values for the slope and vertical velocity are $|h_x| = .01$ and $v = 1 \mu\text{m/hr}$. With the further choices $F = 6.31 \times 10^{17} \text{ atom/m}^2/\text{s}$ and $\nu = 1 \text{ atom/nm}^3$ we get $(1 - \nu v/F) \approx 0.56$, so (16) leads to the condition

$$\tau \left[\alpha + \frac{(3.53 \times 10^{19} \text{ atom/m}^2/\text{s})\beta\tau}{(A + 0.01)} \right] \approx 78.66 . \quad (17)$$

Now let us switch to the dynamics of the model. Not much is known about the time scale of ρ , so we are going to assume

$$\frac{1}{\tilde{\tau}} = g\tilde{\alpha}_1 , \quad (18)$$

where g is a constant factor of order unity. That is, we are assuming that both ρ and h evolve on similar time scales. Note that the quantity $1/\tilde{\tau}$ is the ratio of the monolayer time to the evaporation time. From the above relationship and the definition of $\tilde{\alpha}_1$, we obtain

$$\alpha = \left(\frac{1}{g\tilde{\tau}} \right) \frac{\nu v}{Fa} \sqrt{\frac{D}{\tau}} . \quad (19)$$

Taking ν , v and F as before, and assuming $D \approx 10^{-14} \text{ m}^2/\text{s}$, $a = 1 \text{ nm}$, we get a condition relating α to the other parameters:

$$\alpha \approx \left(\frac{44.03}{g\tilde{\tau}} \right) \tau^{-1/2} . \quad (20)$$

Here the units for α and τ are s^{-1} and s , respectively. Putting (17) and (20) together, we have

$$3.53 \times 10^{19} \frac{\beta}{(A + 0.01)} \approx \left[(78.66)\tau^{-2} - \left(\frac{44.03}{g\tilde{\tau}} \right) \tau^{-3/2} \right] . \quad (21)$$

In order to have a meaningful nucleation term, β must be non-negative, so there is a constraint for the product $g\tilde{\tau}$, namely,

$$g\tilde{\tau} \geq 0.56\sqrt{\tau} . \quad (22)$$

Concerning with the value for τ , there is not much information from experiments. If we take $\tilde{\tau} = 2$, i.e. the evaporation time is twice of the monolayer time, and $g = 1$, then $\tau = 7.2 \text{ s}$, $\alpha = 8.20 \text{ s}^{-1}$ and

$$\frac{\beta}{(A + 0.01)} \approx 1.07 \times 10^{-20} \text{ m}^2/\text{s} . \quad (23)$$

According to the conventional belief, evaporation should be unimportant for usual situations. This is the case if the evaporation length is much longer than the width of a typical step. With our choice for τ , the evaporation length is approximately equal to $0.268 \mu\text{m}$, which is 2.68 times of the typical step width.

Now all the phenomenological parameters in the model are determined except S and A , which thus far are free parameters. We are going to fix them by comparing solutions of the 1-D equations for different combinations of S and A to typical grain shapes. Figs. 4 and 5 show the steady state grain shapes for different values of S , for $A = 3.5 \times 10^{-3}$ and $A = 8.0 \times 10^{-3}$. The calculation was periodic in space, so each figure represents a periodic array of grains. We took $\Delta x = 0.05$, $\Delta t = 0.0025$ for each calculation. The height profiles shown in the figures are plotted relative to the bottom of the valleys. The thick lines in the figures represent a triangular grain with slope equal to 0.01 and they are included in the figures for reference. The size of the grains corresponds approximately to $2.68 \mu\text{m}$ in actual length scale. Simulations show that the steady state mound shapes do not depend on the initial data.

The triangle with slope 0.01 is an useful reference shape because the experimental data show (approximate) slope selection at a slope of this order of magnitude. The figures suggest that the choice $A = 3.5 \times 10^{-3}$ and $S \approx 10^{-7}$ is consistent with such slope selection. This is the regime we use for all our simulations.

The figures also give a lot of useful information about how the solutions depend on A and S . The effect of the “nucleation” term clearly depends on the magnitude of A : if A is small enough, this term works as it should (being mainly active at the peak); but if A is large, it works badly (influencing the slope of the grain everywhere, not just the growth at the peak). For any value of A , the shape of the grain depends strongly on the Schwoebel parameter S . For $S = 0$, the shape is nearly triangular; this is because when there is no uphill current, the adatom density is eventually constant (see Section 5 for further discussion of this point). As S increases, however, the shape becomes rounded and the peak gets higher. This is because larger S amplifies the uphill current, depleting the adatom density in the valleys and enhancing it at the peaks.

Once the value of A is fixed (we use $A = 3.5 \times 10^{-3}$), the value of S can be determined

by matching the coarsening rate of the model to that observed experimentally. This works because the coarsening rate of the model increases monotonically with S (see Sections 4 and 5). If in the experiment, the grains are of order $1\ \mu\text{m}$ after 15-30 minutes, then S should be chosen so that simulations with small random initial height variation coarsen to this size on the same time scale. This occurs for $S \approx 10^{-7}\ \text{m/s}$.

Once the phenomenological parameters in the model are determined, the dimensionless parameters can be calculated and used in the simulations.

4 Phenomenology

The phenomenon of slope selection in the one-dimensional setting is clear from Section 3. Direct simulation of the model shows that slope selection occurs in two-dimensions as well, and the morphology is what we expect: locally conical peaks separated by sharp one-dimensional valleys. When done with random initial data, simulations also reveal coarsening at a rate that depends on S .

Fig. 6 shows the result of a two-dimensional simulation. The number of grid points is 100×100 , which is equivalent to a size of about $1.34\ \mu\text{m}$, in both the x - and y - directions. Periodic boundary conditions are used. The simulation is started with a small random initial height profile and the initial adatom density is equal to zero everywhere. The total time is 500 times the monolayer time, i.e. $500\ t_{ML}$, which is equivalent to 30 minutes in actual time scale. The average height increases linearly in time with a rate equal to the growth rate assumed in Section 3. Grains with very characteristic shapes develop out of the initially random profile. Their slopes and shapes stay roughly invariant as they coarsen.

We have repeated similar simulations for different values of S . When $S = 0$, the system does not coarsen. When $S > 0$, it coarsens steadily until the grain size approaches the size of the period cell – when finite-size effects set in and coarsening ceases. The coarsening rate increases with S , and the morphology is always like that of Fig. 6. Our data on the coarsening rate is summarized in Fig. 7, which gives the standard deviation of the height as a function of time.

To gain additional insight about the coarsening, it is convenient to consider the one-

dimensional case. In this setting, we can simulate much larger systems, with many more generations of coarsening before the onset of finite-size effects. Fig. 8 shows the evolution of a one-dimensional system starting with random initial height and zero surface adatom density. The system size is equal $13.4 \mu\text{m}$ in actual length scale and the total number of grid points is 1000. Periodic boundary conditions are used. The total time is $600 t_{ML}$, which corresponds to 36 minutes in actual time scale.

The bottom profile in Fig. 8 is the initial condition. The other profiles show the height of the film at a sequence of evenly spaced times.³ The figure shows clearly the phenomenon of shape selection and coarsening. One can also see the coarsening process, in which small grains disappear and large grains become larger. We shall study this process further in Section 5.

Fig. 9 shows the average surface roughness (averaged over 100 different random initial profiles) of our one-dimensional simulation and Fig. 10 shows its rate of change. There is a long initial transient, during which the coarsening rate increases roughly linearly in time, until it saturates around $500 t_{ML}$. After that, the coarsening rate appears to be roughly constant.

5 The sources of slope selection and coarsening

We have shown, by direct numerical simulation, that our model exhibits slope selection and coarsening. It remains to explain why. This section elucidates the underlying mechanisms. Our arguments are mainly heuristic rather than rigorous. We believe that they are nevertheless enlightening.

5.1 Slope selection

The essence of slope selection is easy to understand. The adatom density is nearly constant, varying in space and time by just a few percent (see Sections 5.2 and 5.3). If we ignore this variation and treat ρ as a constant, then our h -equation basically specifies the horizontal

³For graphical clarity, Fig. 8 shows not $h(x, t_j)$, but rather $h(x, t_j) - ct_j$, where c is a suitable constant. It has been checked that h_{\min} grows linearly in time.

velocity of the steps (through ϕ_{attach}) and the vertical velocity of the peaks (through ψ_{nucl}). These determine a unique slope: if the horizontal velocity is $h_t/|\nabla h| = \phi$ and the peak velocity is $h_t = \psi$, then the slope is $|\nabla h| = \psi/\phi$.⁴ In this “geometric” approximation, the profile of h near each peak x_i becomes a growing cone, and the surface of the film is the envelope of these cones:

$$\begin{aligned} h(x, t) &= \max_i \left(\psi t - \frac{\psi}{\phi} |x - x_i| \right) \\ &= \psi t - \frac{\psi}{\phi} h_*(x) \end{aligned} \quad (24)$$

where $h_*(x) = \min_i \{|x - x_i|\}$. This geometrical solution is shown schematically in Fig. 11.

This is essentially the “geometrical model” of spiral growth explored in [20]. Our situation is slightly different: the evolution of h is specified by PDE’s rather than geometry, and ρ is not exactly constant. So the profile of h is not exactly conical, and slope-selection is approximate rather than exact. But these differences are minor; the physical mechanism of slope selection is captured concisely by the geometric model.

In our numerical simulations, the mean height grows linearly in time, with essentially no scatter. The formula (24) explains why: to the extent that this geometrical model is accurate, h_t is identically equal to ψ .

5.2 Coarsening

The geometric model (24) does not coarsen. In fact, its spatial structure is given by $h_*(x) = \min_i \{|x - x_i|\}$, and its valleys are given by the Voronoi diagram of the peaks. So the origin of coarsening lies in *deviations* from the geometric model.

The argument leading to (24) ignored the spatial variation of the adatom density. But ρ is not exactly constant: if $S > 0$, then the uphill current depletes the valleys and enriches the peaks. Thus the variation of the adatom density reflects the topography of the film: ρ

⁴If $\rho = \rho_0$ is constant, then h solves the *Hamilton-Jacobi* equation: $\nu h_t = \alpha \rho_0 |\nabla h| + \beta \rho_0^2 / (A + |\nabla h|)$. Its solution is not exactly piecewise linear in 1-D, nor exactly a cone in 2-D. But the solution is nevertheless well-approximated by a piecewise linear function in 1-D and a cone in 2-D. Figs. 4 and 5 confirm the 1-D version of this assertion (note that ρ being constant corresponds to S being zero). Of course, the horizontal velocity is not really $\phi_{\text{attach}}/\nu = \alpha \rho_0/\nu$, but rather $h_t/|\nabla h| = \frac{1}{\nu} \phi_{\text{attach}} + \frac{1}{\nu} \psi_{\text{nucl}}/|\nabla h| = \alpha \rho_0/\nu + \beta \rho_0^2/\nu (A + |\nabla h|) |\nabla h|$.

is lowest at the valleys and highest at the peaks. This variation is moreover nonuniform: ρ is smaller at peaks associated with smaller grains, since they have smaller catchment areas.

These topography-driven variations in ρ are what drive the coarsening. Indeed, our nucleation term ψ_{nucl} is an increasing function of ρ . Since the smallest grains have the smallest peak values of ρ , they also have the smallest vertical velocities. They are eventually eliminated by their larger neighbors, which grow faster.

To see this coarsening mechanism numerically, it is convenient to consider the one-dimensional version of our model. Figs. 12 and 13 show a simulation with periodic boundary conditions, in which an initial profile with two peaks coarsens into a profile with a single peak. Fig. 12 shows the graph of $h(x, t)$ at several evenly-spaced times⁵, and Fig. 13 shows the graph of $\rho(x, t)$ at the same times.⁶ (The curves having the same color indicate the corresponding quantities at the same time.) Looking at h one sees that there is a selected slope, and the vertical velocity of the larger peak is nearly constant. The vertical velocity of the smaller peak is smaller, however, and it decreases significantly as the associated grain becomes smaller. Eventually the valleys merge, eliminating the smaller peak and its associated grain. Looking at ρ , one sees that the mechanism is essentially as described above: the smaller grain has a lower peak value of ρ , which decreases as time proceeds, slowing down the vertical growth of the peak. In addition, the figure shows a point we did not mention above: as the smaller grain shrinks, the value of ρ decreases not just at the peak but *throughout*; as the larger grain grows, the value of ρ also increases *throughout*. This effect increases the difference between the horizontal growth rates as well as the difference between the vertical growth rates – accelerating the disappearance of the smaller grain.

Our analysis of the coarsening mechanism suggests a linear coarsening law for random initial data, consistent with the numerical observations reported in Section 4. In fact, making the usual approximation that $|h_x|$ is constant, the spatial variation of the right hand side of the h -equation

$$\nu h_t = \alpha \rho |\nabla h| + \frac{\beta}{(A + |\nabla h|)} \rho^2$$

is entirely due to ρ . This variation is stochastic, because it reflects the local topography; but

⁵For graphical clarity, we are actually plotting $h(x, t_j) - ct_j$ where c is a suitable constant.

⁶The graph for ρ at $t = 0$ is omitted since it is equal to zero everywhere.

its overall magnitude should be stationary once the mean grain size is large enough. Thus if h_{peak} is the typical height of a peak and h_{valley} is the typical height of a valley then

$$h_{\text{peak}} - h_{\text{valley}} \text{ should grow linearly in } t, \text{ when } t \text{ is large.}$$

But we also believe

$$\text{the slope } |\nabla h| \text{ is essentially fixed.}$$

The two statements are consistent only if the typical length scale grows linearly in time.

The coarsening mechanism discussed above is different from – but related to – the one considered by Schulze and Kohn in [20]. That paper explored the consequences of peak-structure heterogeneity. Rather than specify a single peak velocity ψ , it took the vertical velocity ψ_i of the i th peak to be random (chosen independently for each i from a suitable probability distribution). Such heterogeneity induces coarsening, because faster-growing peaks tend to dominate. The coarsening observed in the present context is similar – except that the heterogeneity arises from local topography and the uphill current, rather than from structural differences in the peaks.

5.3 The dependence on S .

We saw in Section 4 that the coarsening rate depends mainly on S , the coefficient of the uphill current. To explain this observation, consider once again the one-dimensional version of our model. It is clear from Fig. 13 that the profile of ρ changes slowly in time, determined mainly by the evolution of h , except for fast transients when valleys merge and peaks disappear. So we can understand the spatial structure of ρ by considering the *stationary* ρ -equation

$$(D\rho_x - S\rho h_x)_x - \alpha\rho|h_x| - \frac{\beta}{(A + |h_x|)}\rho^2 - \frac{\rho}{\tau} + F = 0 . \quad (25)$$

We assume as usual that the deposition rate F is constant.

Due to slope selection, $|h_x|$ is nearly constant, with h_x changing sign at peaks and valleys – which are sharp, due to the absence of a diffusive term in the h -equation. We shall, as an approximation, ignore the spatial variation of $|h_x|$, treating the height profile as a piecewise linear function with discontinuous slope.

The adatom density must be continuous at the peaks and valleys. So the terms involving α and β are continuous. But $S(\rho h_x)_x$ is singular: it behaves like a delta-function at each peak and valley, with weight $S\rho[h_x]$. (Here $[h_x]$ denotes the jump in h_x .) Since the net singularity must be zero, $D\rho_{xx}$ must also be singular – in other words ρ_x must jump – and

$$D[\rho_x] = S\rho[h_x] \tag{26}$$

at each peak or valley. If in addition the distance between peaks and valleys is large, then ρ will decay to a far-field value ρ_∞ away from the peaks and valleys. The value of ρ_∞ is easily determined from (25) by setting $\rho_x = \rho_{xx} = h_{xx} = 0$:

$$-\alpha\rho_\infty|h_x| - \frac{\beta}{(A + |h_x|)}\rho_\infty^2 - \frac{\rho_\infty}{\tau} + F = 0 .$$

The profile of ρ is sketched in Fig. 14.

We can now explain the numerical observation that the coarsening rate depends strongly on S , with no coarsening at all if $S = 0$. Recall from subsection 5.2 that coarsening is driven by the deviations of ρ at the peaks and valleys. But *the deviations of ρ are driven by the uphill current, through the jump condition* (26). If there is no uphill current – that is, if $S = 0$ – then ρ is identically equal to ρ_∞ , and there is no coarsening. As one increases the value of S , one effectively increases the value of $[\rho_x] = (S\rho/D)[h_x]$, which in turn increases the deviations of ρ .

In truth, the distance between peaks and valleys is rarely large enough for ρ to reach its asymptotic value ρ_∞ ; compare, for example, Figs. 13 and 14. But the main features of our analysis apply regardless of the distance between the peaks and valleys: $S = 0$ implies $\rho = \rho_\infty$, and increasing S increases the deviations of ρ at the peaks and valleys.

6 Discussion

We have presented a novel approach to epitaxial growth, based on a coupled system of PDE's for the surface height h and the surface adatom density ρ . This model is appropriate for spiral growth, and more generally for any situation where the crystal is stepped and nucleation occurs only at peaks. Our numerical simulations show slope-selection and coarsening, with

a coarsening rate that depends mainly on the strength of the uphill current. Our analysis reveals that the mechanism of slope selection is essentially geometric: the selected slope is the ratio of the typical peak velocity to the typical step velocity. Coarsening, on the other hand, has a different, more stochastic origin: it comes from spatial fluctuations in the adatom density, which arise through interaction of the uphill current and local topography.

Slope selection is not limited to spiral growth. In fact, this phenomenon often accompanies kinetic roughening. Such slope selection is commonly modeled using a scalar fourth-order equation such as

$$h_t = \nabla \cdot [(|\nabla h|^2 - k) \nabla h] - \epsilon \Delta^2 h + F , \quad (27)$$

see e.g. [8, 9, 19]. Anisotropic analogues of (27) have also been considered [12, 14]. To explain why (27) produces slope selection, we observe that $\tilde{h} = h - Ft$ performs steepest descent for

$$\int \left[\frac{1}{4} (|\nabla h|^2 - k)^2 + \frac{\epsilon}{2} |\nabla \nabla h|^2 \right] dx . \quad (28)$$

Considering large time and length scales is equivalent, by scaling, to considering the behavior as $\epsilon \rightarrow 0$. Away from peaks and valleys the term $(|\nabla h|^2 - k)^2$ dominates, effectively setting the value of $|\nabla h|$ to the “magic slope” $k^{1/2}$. This approach to slope selection is quite different from ours.

There is however an important point of contact between our viewpoint and the literature on kinetic roughening, namely the role of the Ehrlich-Schwoebel barrier in producing an uphill current. The recent papers of Amar and Family are particularly relevant [39, 40, 41]. This work uses an atomic-scale model of a stepped crystal to evaluate the mean uphill current (due to the Ehrlich-Schwoebel barrier) and the mean downhill current (due to “cascading” of adatoms as they land on the crystal). Then it predicts the selected slope by requiring that the net current vanishes. Our approach is similar in spirit, but different in two significant details: (a) our downhill current is due to large-scale diffusion rather than cascading; and (b) we set the *divergence* of the net adatom current to zero, rather than requiring this current to vanish pointwise.

The difference between our model and that of [39, 40, 41] can also be seen another way. Our model is perturbative around $S = 0$; slope selection is a zeroth order effect (present even for $S = 0$), while coarsening is a first order effect (driven by the spatial variation of ρ

induced by $S \neq 0$). In [39, 40, 41], by contrast, slope selection is a first order effect: without an uphill current, the flat film is stable and there is no kinetic roughening.

Most models of kinetic roughening take the view that desorption is negligible, leading to scalar fourth-order models of the form $h_t = -\nabla \cdot J + F$ like Eqn. (27). An exception is the recent paper [13], which argues that desorption, though small, has an essential effect on morphology because it occurs mainly at the peaks. This leads to consideration of the continuum model

$$h_t = \nabla \cdot [(|\nabla h|^2 - k)\nabla h] - \epsilon \Delta^2 h + V(|\nabla h|), \quad (29)$$

where $V(|\nabla h|)$ is a monotone function of the slope, minimized at the peaks (where $|\nabla h| = 0$). The simulations in [13], based on (29), show phenomenology remarkably similar to that of our model, though the details (in particular, the coarsening law) are different. Perhaps the source of this similarity is the analogy between our nucleation term and the term $V(|\nabla h|)$ in (29).

Models similar to (27) display coarsening, see e.g. [8, 9, 12, 14, 19]. In fact an equation very similar to (27) has been discussed as a model for coarsening during spiral growth [19]. The effects that drive the coarsening of (27) are very different from those in our model. Indeed, the Liapunov functional (28) assigns a “defect energy” to the valleys of h , which represent grain boundaries [14, 43]. The solution of (27) coarsens to reduce this defect energy by increasing the overall length scale. Our model is entirely different – it is dominated by the velocities of the peaks rather than the defect energy of the valleys.

Our approach and that of [19] address different physical mechanisms of coarsening. Not surprisingly, they also make different predictions. Under our model surface roughness grows roughly linearly in time, whereas under (27) it grows like $t^{1/3}$. The experimental data on spiral growth in YBCO are not, to our knowledge, capable of distinguishing between the two models. In truth, these different approaches are not necessarily exclusive: the physics of coarsening in YBCO could easily involve features of both.

Acknowledgements

This work was supported by DARPA and NSF. We are indebted to Weinan E and Tim

Schulze for many useful discussions. We also thank the anonymous referee for helpful suggestions and references.

References

- [1] Burton, W.K., Cabrera, N. and Frank, F.C., The growth of crystals and the equilibrium structure of their surfaces, *Phil. Trans. Roy. Soc. Lond.* **243A**, 1951, 299-358.
- [2] Chernov, A.A., Formation of crystals in solutions, *Contemp. Phys.* **30**, 1989, 251-276.
- [3] Van Der Eerden, J.P., Crystal growth mechanisms, in *Handbook of Crystal Growth 1*, edited by D.T.J. Hurle, North-Holland, 1993, 311-475.
- [4] Pimpinelli, A. and Villain, J., *Physics of Crystal Growth*, Cambridge University Press, 1998.
- [5] Villain, J., Continuum models of crystal-growth from atomic-beams with and without desorption, *J. de Physique I* **1**, 1991, 19-42.
- [6] Vvedensky, D.D., Zangwill, A., Luse, C.N., and Wilby, M.R., Stochastic equations of motion for epitaxial growth, *Phys. Rev. E* **48**, 1993, 852-862.
- [7] Hunt, A.W., Orme, C., Williams, D.R.M., Orr, B.G., and Sander, L.M., Instabilities in MBE growth, *Europhys. Lett.* **27**, 1994, 611-616.
- [8] Siegert, M. and Plischke, M., Slope selection and coarsening in molecular beam epitaxy, *Phys. Rev. Lett.* **73**, 1994, 1517-1520.
- [9] Siegert, M., Ordering dynamics of surfaces in molecular beam epitaxy, *Physica A* **239**, 1997, 420-427.
- [10] Krug, J., Origins of scale invariance in growth processes, *Adv. Phys.* **46**, 1997, 139-282.
- [11] Levi, A.C. and Kotrla, M., Theory and simulation of crystal growth, *J. Phys.-Cond. Matter* **9**, 1997, 299-344.

- [12] Siegert, M., Coarsening dynamics of crystalline thin films, *Phys Rev. Lett.* **81**, 1998, 5481-5484.
- [13] Šmilauer, P., Rost, M., and Krug, J., Fast coarsening in unstable epitaxy with desorption, *Phys. Rev. E* **59**, 1999, R6263-R6266.
- [14] Moldovan, D. and Golubovic, L., Interfacial coarsening dynamics in epitaxial growth with slope selection, *Phys. Rev. E* **61**, 2000, 6190-6214.
- [15] Chernov, A.A., The spiral growth of crystals, *Sov. Phys. Uspekhi* **4**(1), 1961, 116-148.
- [16] Karma, A. and Plapp, M., Spiral surface growth without desorption, *Phys Rev. Lett.* **81**, 1998, 4444-4447.
- [17] Smereka, P., Spiral crystal growth, *Physica D* **138** (3-4), 2000, 282-301.
- [18] Aranson, I.S., Bishop, A.R., Daruka, I. and Vinokur, V.M., Ginzburg-Landau theory of spiral surface growth, *Phys. Rev. Lett.* **80**, 1998, 1770-1773.
- [19] Ortiz, M., Repetto, E. and Si, H., A continuum model of kinetic roughening and coarsening in thin films, *J. Mech. Phys. Solids* **47** (4), 1999, 697-730.
- [20] Schulze, T.P. and Kohn, R.V., A geometric model for coarsening during spiral-mode growth of thin films, *Physica D* **132**, 1999, 520-542.
- [21] Raistrick, I.D. and Hawley, M., Scanning tunneling and atomic force microscope studies of thin sputtered films of $\text{YBa}_2\text{Cu}_3\text{O}_{7-\delta}$, in *Interfaces in High- T_c Superconducting Systems*, edited by S.L. Shindé and D.A. Rudman, Springer-Verlag, 1994, 28-70.
- [22] Schlom, D.G., Anselmetti, D., Bednorz, J.G., Gerber, Ch. and Mannhart, J., Epitaxial growth of cuprate superconductors from the gas phase. *J. Cryst. Growth* **137**, 1994, 259-267.
- [23] Yeadon, M., Aindow, M., Wellhöfer, F. and Abell, J.S., Topographical development and misfit relief in laser-ablated heteroepitaxial $\text{YBa}_2\text{Cu}_3\text{O}_{7-\delta}$ thin films, *J. Cryst. Growth* **172**, 1997, 145-155.

- [24] Blank, D.H.A., Bijlsma, M.E., Moerman, R., Rogalla, H., Stork, F.J.B. and Roshko, A., Surface roughness and height-height correlation dependence on thickness of YBaCuO thin films, *J. Alloys Compounds* **251**, 1997, 31-33.
- [25] Schulze, T.P. and E, W., A continuum model for epitaxial growth, *J. Cryst. Growth* **222**, 2001, 414-425.
- [26] E, W. and Yip, N.K., Continuum theory of epitaxial crystal growth, *J. Stat. Phys.* **104**, 2001, 221-253.
- [27] Ehrlich, G. and Hudda, F.G., Atomic view of surface self-diffusion: tungsten on tungsten, *J. Chem. Phys.* **44**, 1966, 1039-1049.
- [28] Schwoebel, R.L. and Shipsey, E.J., Step motion on crystal surfaces, *J. Appl. Phys.* **37**, 1966, 3682-3686; Schwoebel, R.L., Step motion on crystal surfaces. II, *J. Appl. Phys.* **40**, 1969, 614-618.
- [29] Lo, T.S. and Kohn, R.V., Modeling MOCVD growth of YBCO thin films, in *Growth, Evolution and Properties of Surfaces, Thin Films and Self-Organized Structures*, edited by S.C. Moss, MRS Symposia Proceedings Vol. 648, 2001, P6.49
- [30] Guyer, J.E. and Voorhees, P.W., Morphological stability and compositional uniformity of alloy thin films, *J. Cryst. Growth* **187**, 1998, 150-165.
- [31] Leonard, F. and Desai, R.C., Alloy decomposition and surface instabilities in thin films, *Phys. Rev. B* **57**, 1998, 4805-4815.
- [32] Spencer, B.J., Voorhees, P.W. and Tersoff, J., Enhanced instability of strained alloy films due to compositional stresses, *Phys. Rev. Lett.* **84**, 2000, 2449-2452.
- [33] Yu, Y.-K. and Wille, L.T., A continuum approach to two-component thin film growth, in *Mechanisms and Principles of Epitaxial Growth in Metallic Systems*, edited by L.T. Wille *et al.*, Symposium Volume 528, Materials Research Society, 1998, 83-90.
- [34] Osher, S. and Sethian, J.A., Front propagation with curvature-dependent speed: algorithms based on Hamilton-Jacobi formulations, *J. Comp. Phys.* **79**, 1988, 12-49.

- [35] Sethian, J.A., *Level Set Methods: Evolving Interfaces in Geometry, Fluid Mechanics, Computer Vision, and Materials Science*, Cambridge University Press, 1st Ed., 1996.
- [36] Gyure, M., Ratsch, C., Merriman, B., Caffisch, R., Osher, S., Zinck, J. and Vvedensky, D., Level set method for the simulation of epitaxial phenomena, *Phys. Rev. E* **58**, 1998, R6927-R6930.
- [37] Evans, L.C., *Partial Differential Equations*, American Mathematical Society, 1998.
- [38] Frank, F.C., On the kinematic theory of crystal growth and dissolution processes. In *Growth and Perfection of Crystals*, edited by R.H. Doremus, *et al.*, Chapman & Hall, 1958, 411-419.
- [39] Amar, J.G. and Family, F., Critical temperature for mound formation in molecular-beam epitaxy, *Phys. Rev. B* **54**, 1996, 14071-14076.
- [40] Amar, J.G. and Family, F., Step-adatom attraction as a new mechanism for instability in epitaxial growth, *Phys. Rev. Lett.* **77**, 1996, 4584-4587.
- [41] Amar, J.G. and Family, F., Effects of crystalline microstructure on epitaxial growth, *Phys. Rev. B* **54**, 1996, 14742-14753.
- [42] Press, W.H., Flannery, B.R., Teukolsky, S.A., and Vetterling, W.T., *Numerical Recipes: The Art of Scientific Computing*, Cambridge University Press, 1986.
- [43] Jin, W. and Kohn R.V., Singular perturbation and the energy of folds, *J. Nonlinear Sci.* **10**, 2000, 355-390.

Figure captions

Fig. 1. Schematic of steps and terraces.

Fig. 2. Schematic of h as a smooth function interpolating step positions.

Fig. 3. Schematic of diffusion and attachment on a steady step train. Adatoms arrive at constant rate F . In the middle of a terrace, an adatom hops left or right with equal probabilities. At the bottom of a step, an adatom may attach to the film or may hop to either neighboring terrace. At the top of a step, an adatom may hop to either neighboring terrace. Hopping rates must be chosen to satisfy detailed balance. The Ehrlich-Schwoebel barrier makes hopping across steps difficult, and inhibits attachment from the top of a step.

Fig. 4. Steady state grain shape for $A = 3.5 \times 10^{-3}$.

Fig. 5. Steady state grain shape for $A = 8.0 \times 10^{-3}$.

Fig. 6. Coarsening in two-dimensions.

Fig. 7. Coarsening rates for different values for S .

Fig. 8. Coarsening in one dimension.

Fig. 9. Average surface roughness vs time.

Fig. 10. Average coarsening rate vs time.

Fig. 11. Schematic of the geometrical solution.

Fig. 12. Competition between two grains in 1-D.

Fig. 13. Evolution of $\rho(x, t)$ during coarsening.

Fig. 14. Sketches of profiles of ρ : (a) for small S , and (b) for larger S .

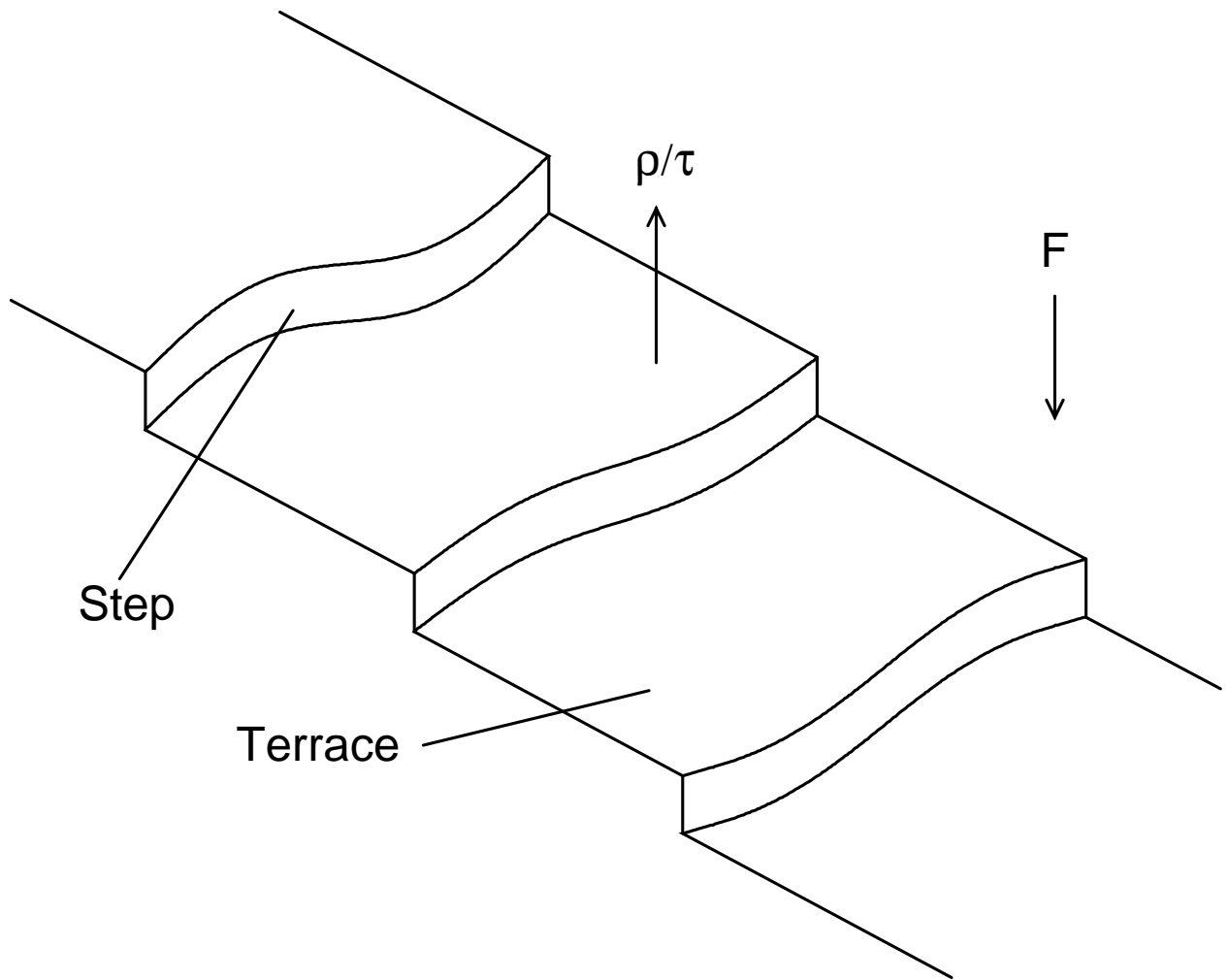


Fig. 1.

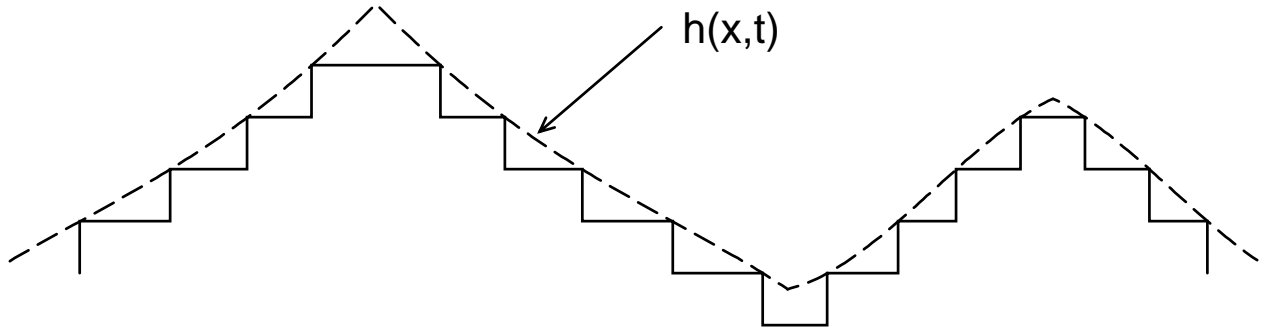


Fig. 2.

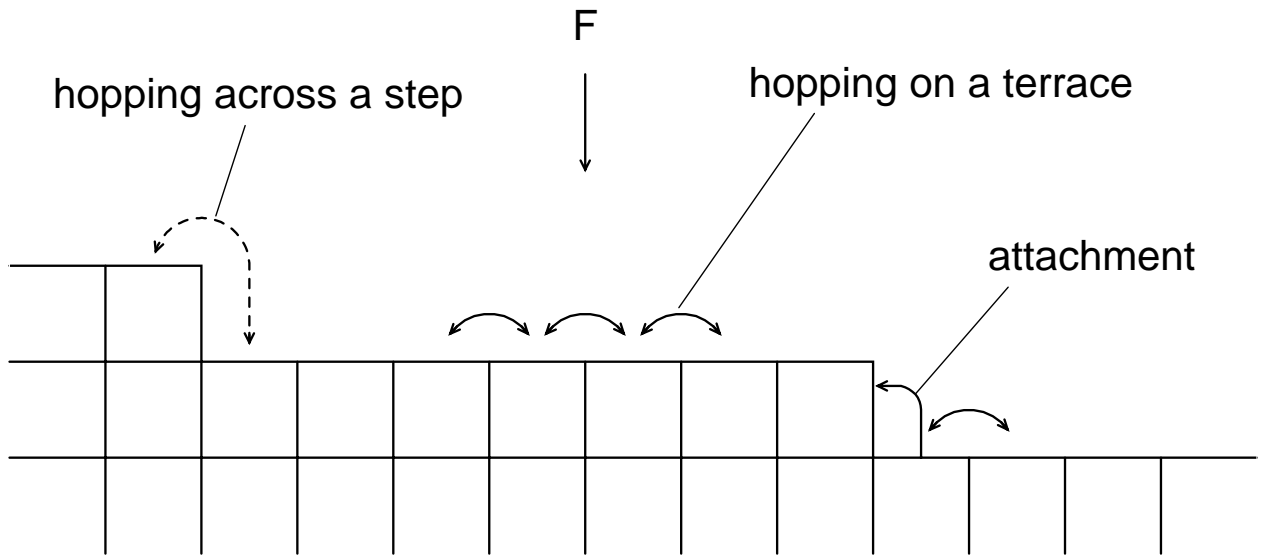


Fig. 3.

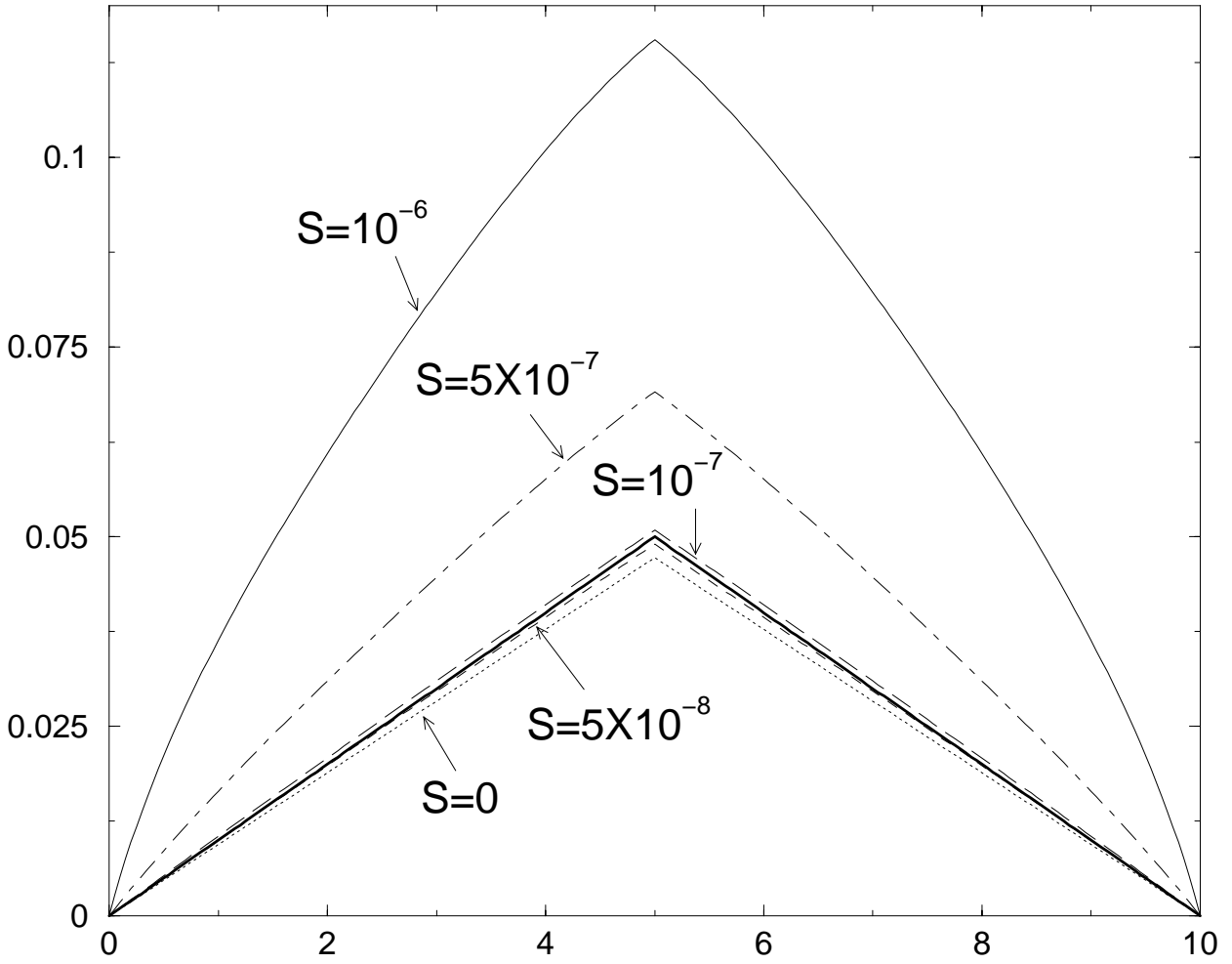


Fig. 4

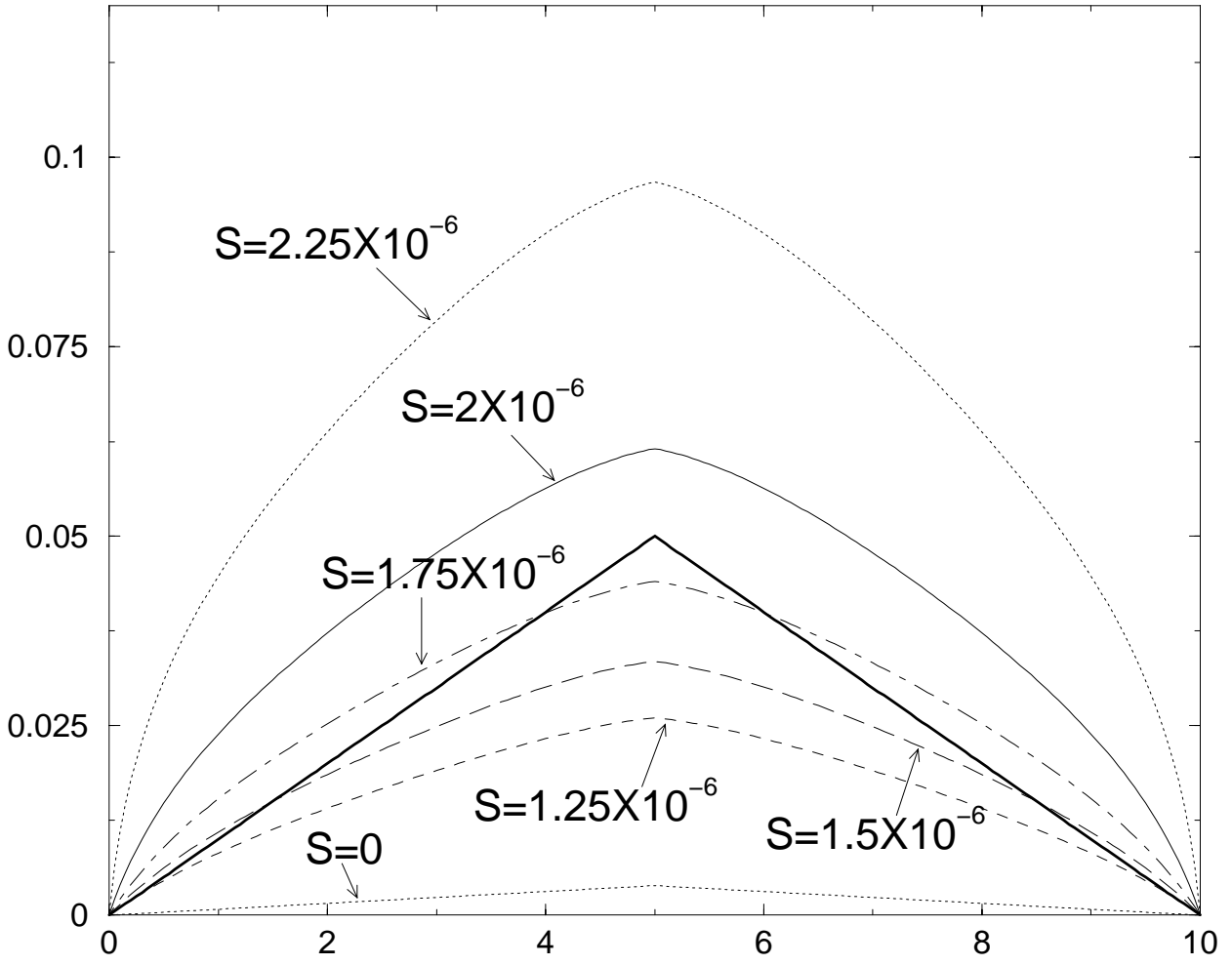


Fig. 5

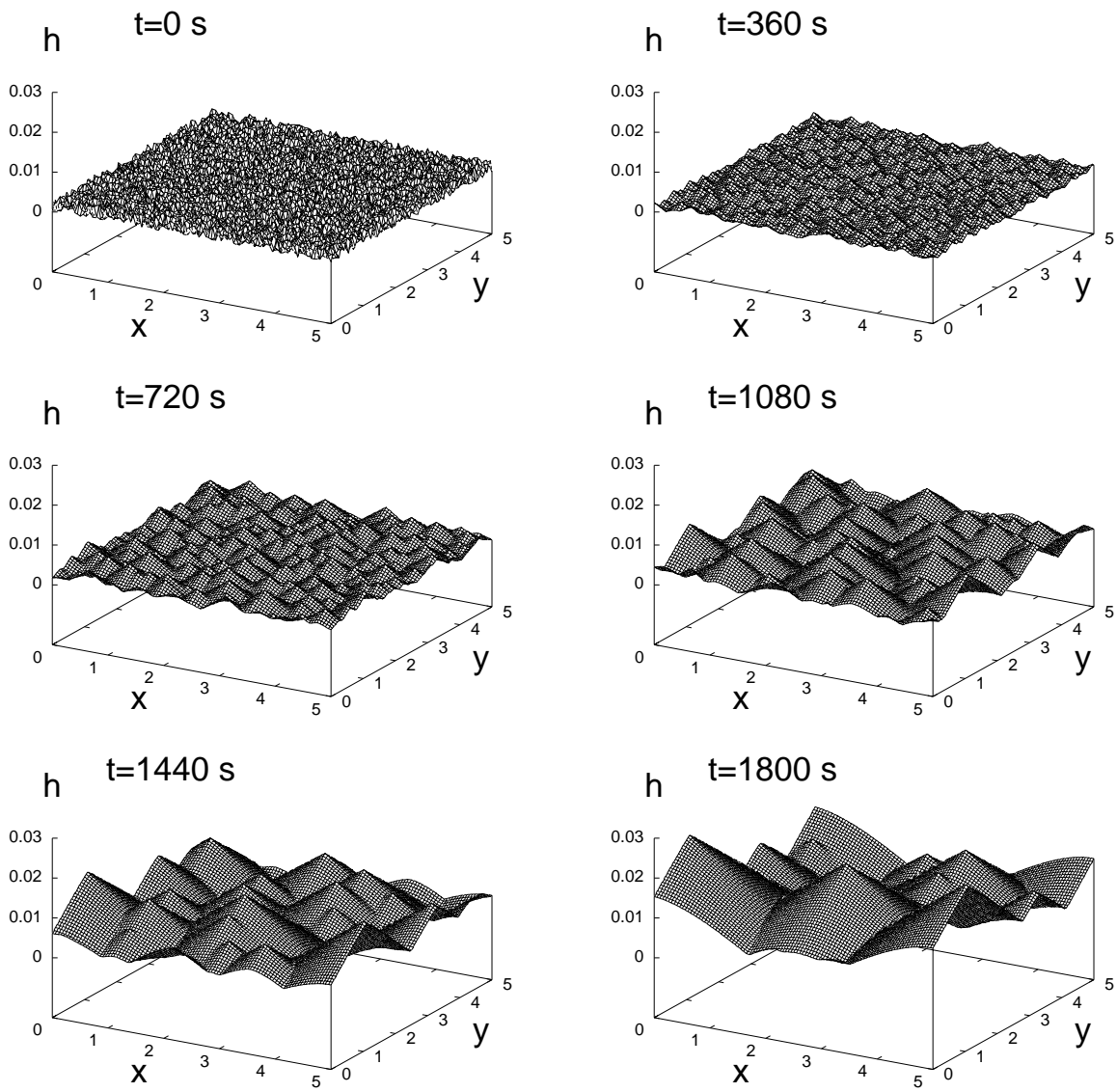


Fig. 6

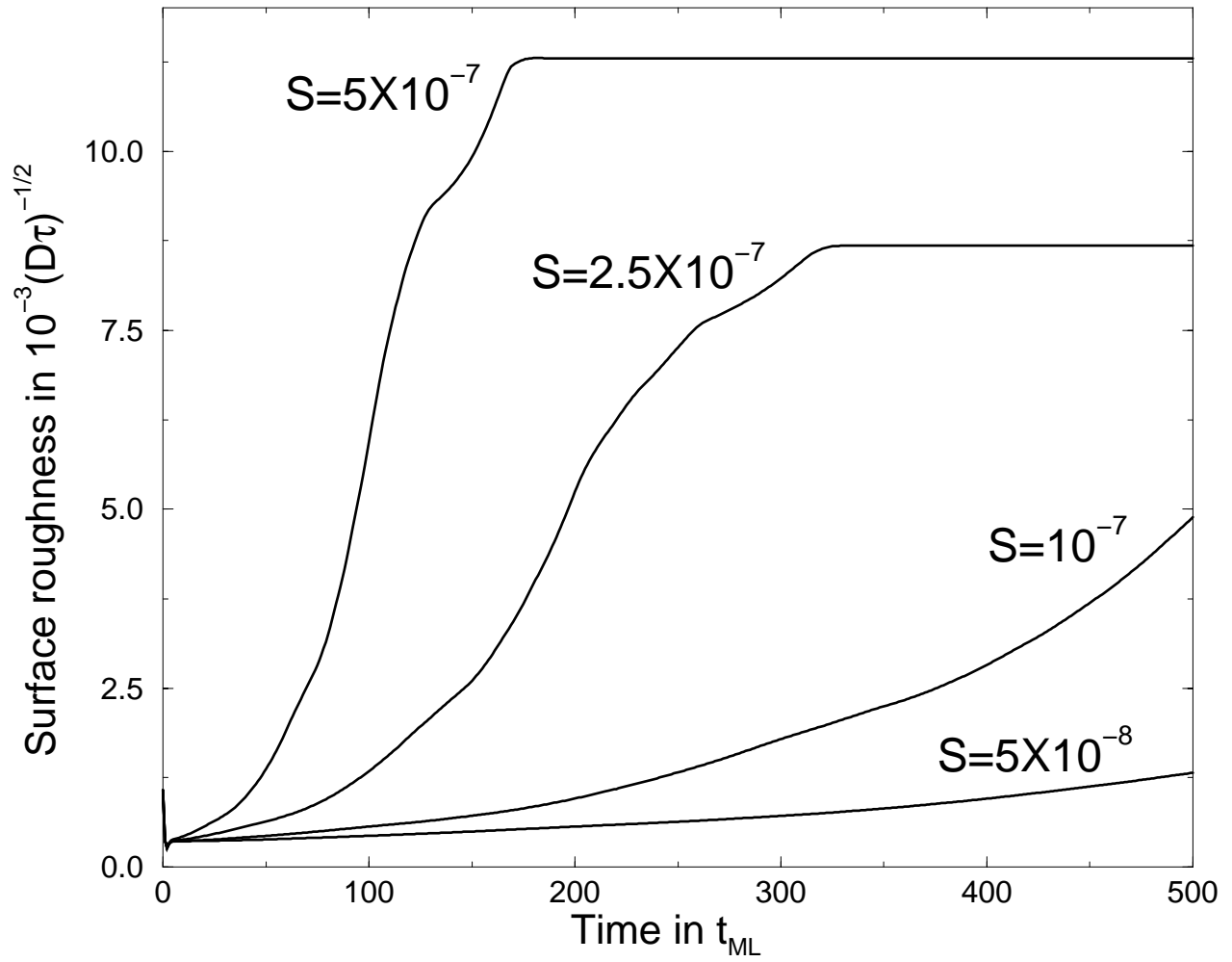


Fig. 7

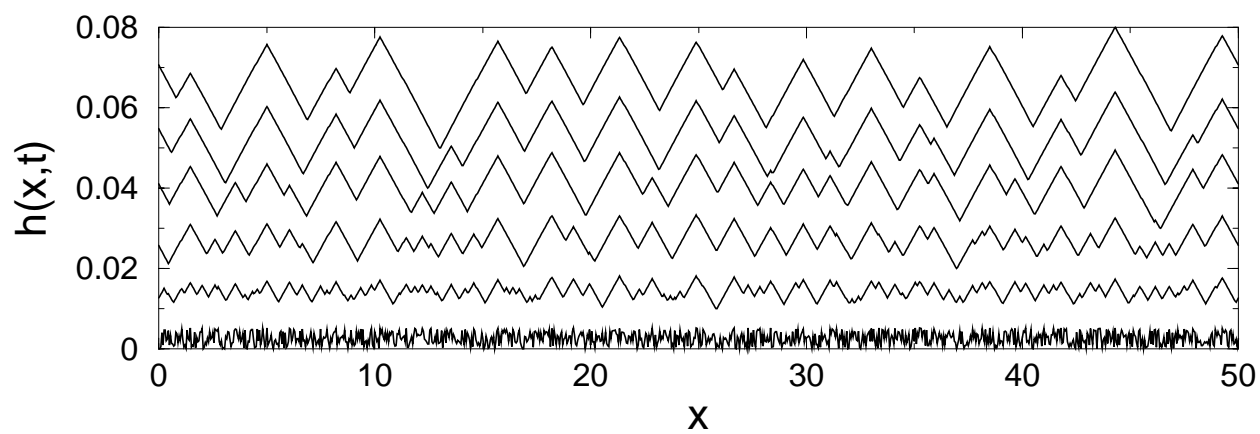


Fig. 8

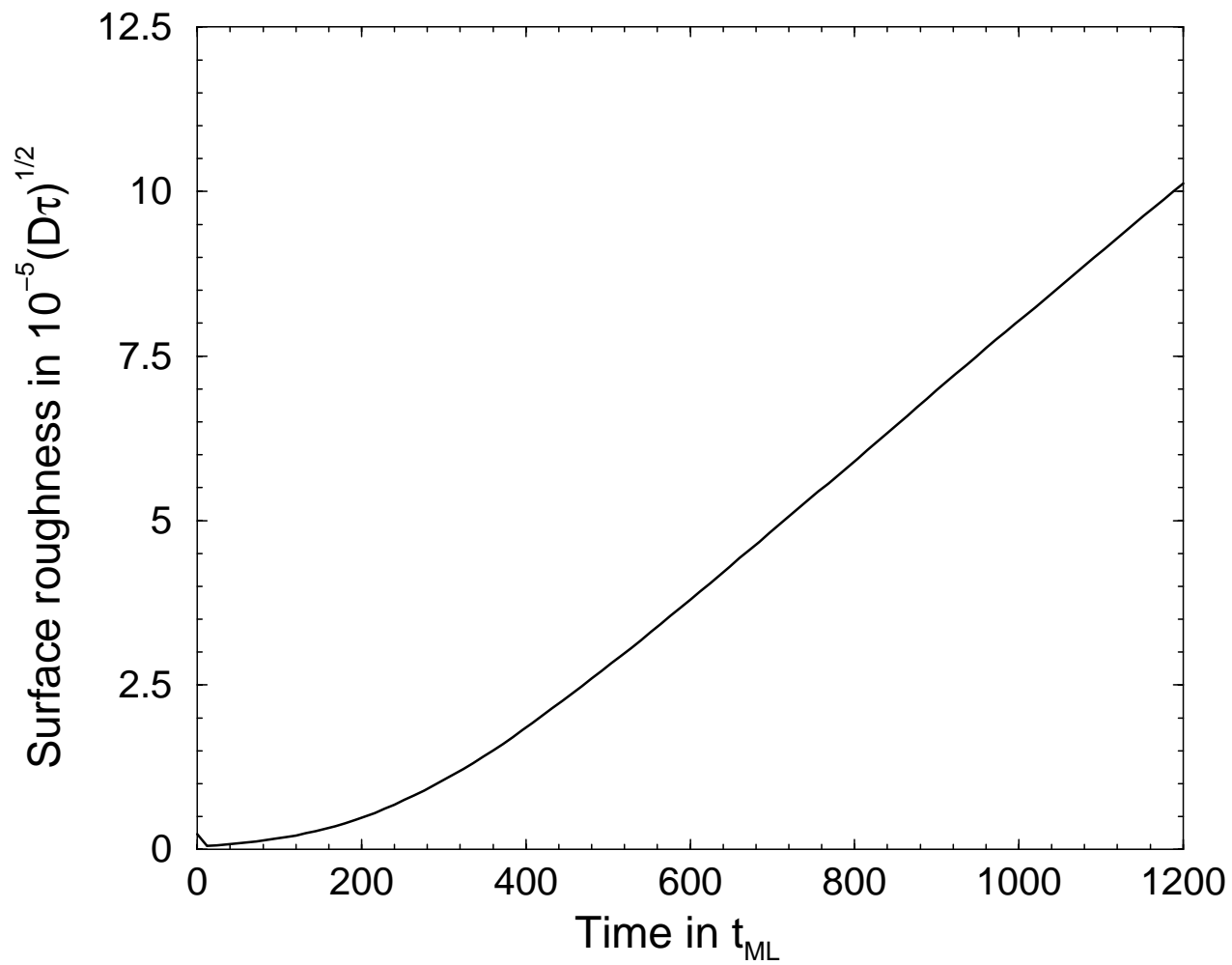


Fig. 9

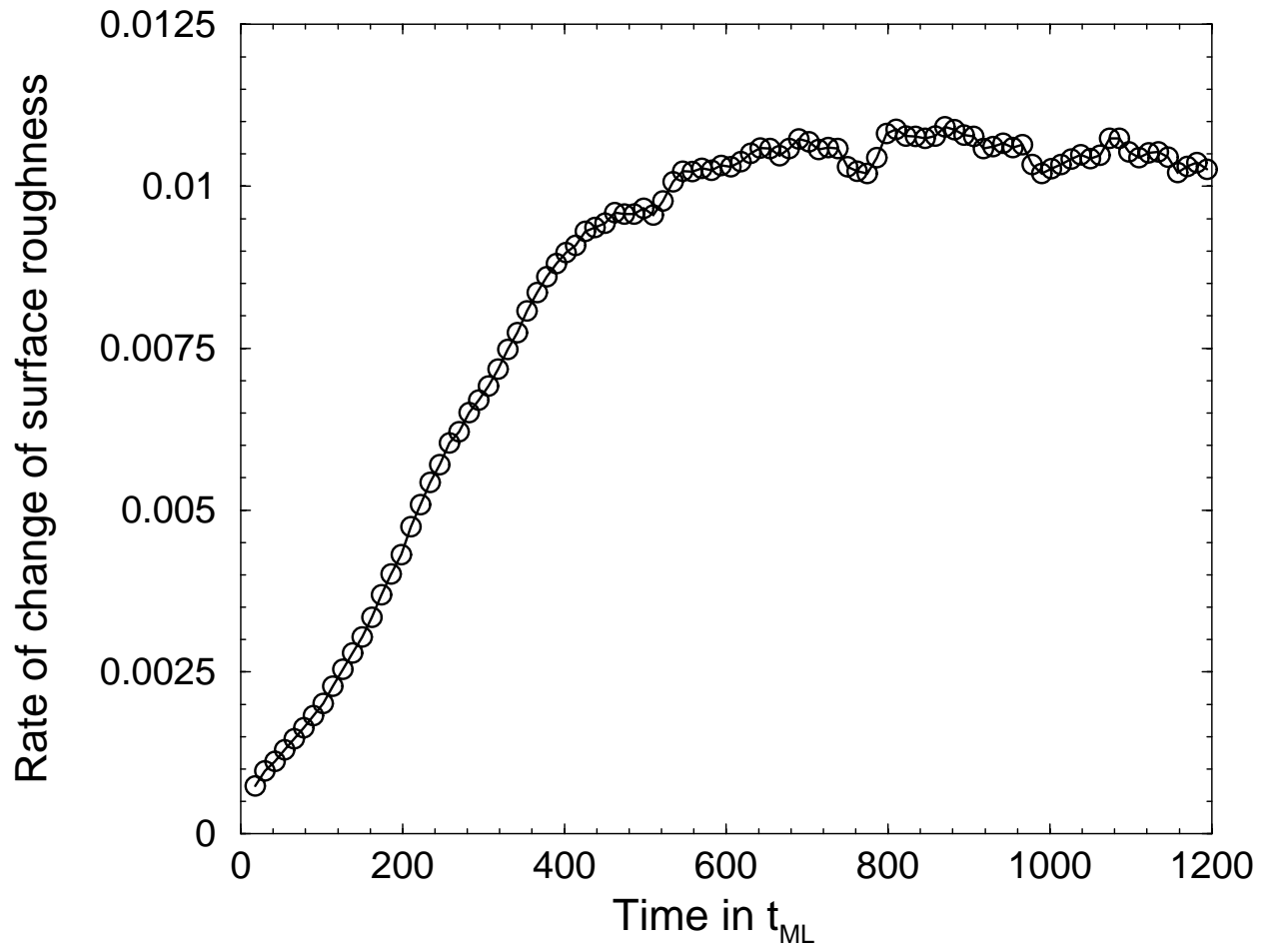


Fig. 10

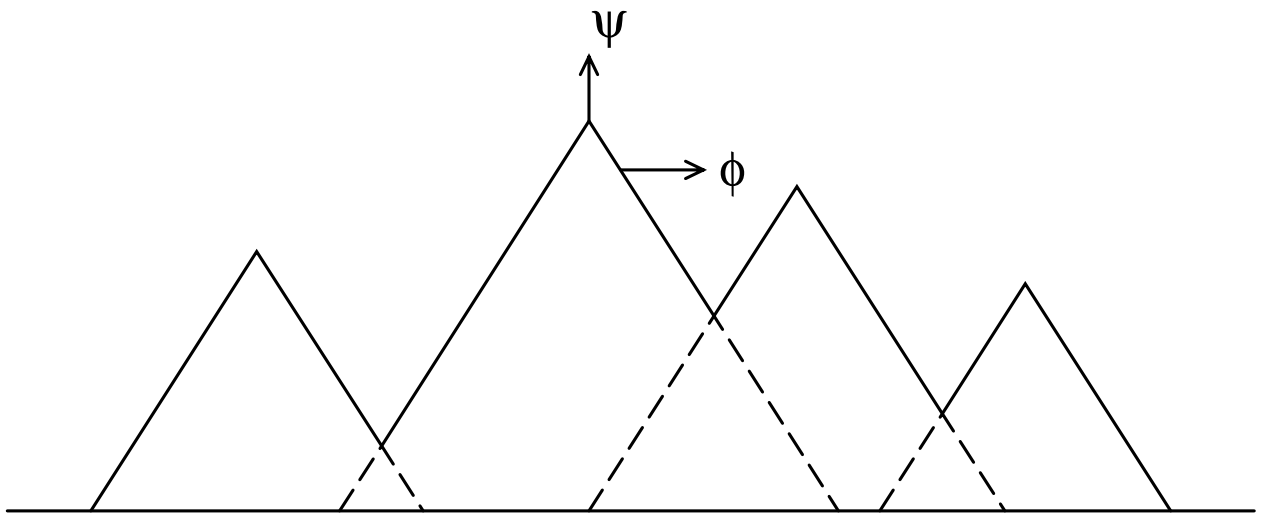


Fig. 11

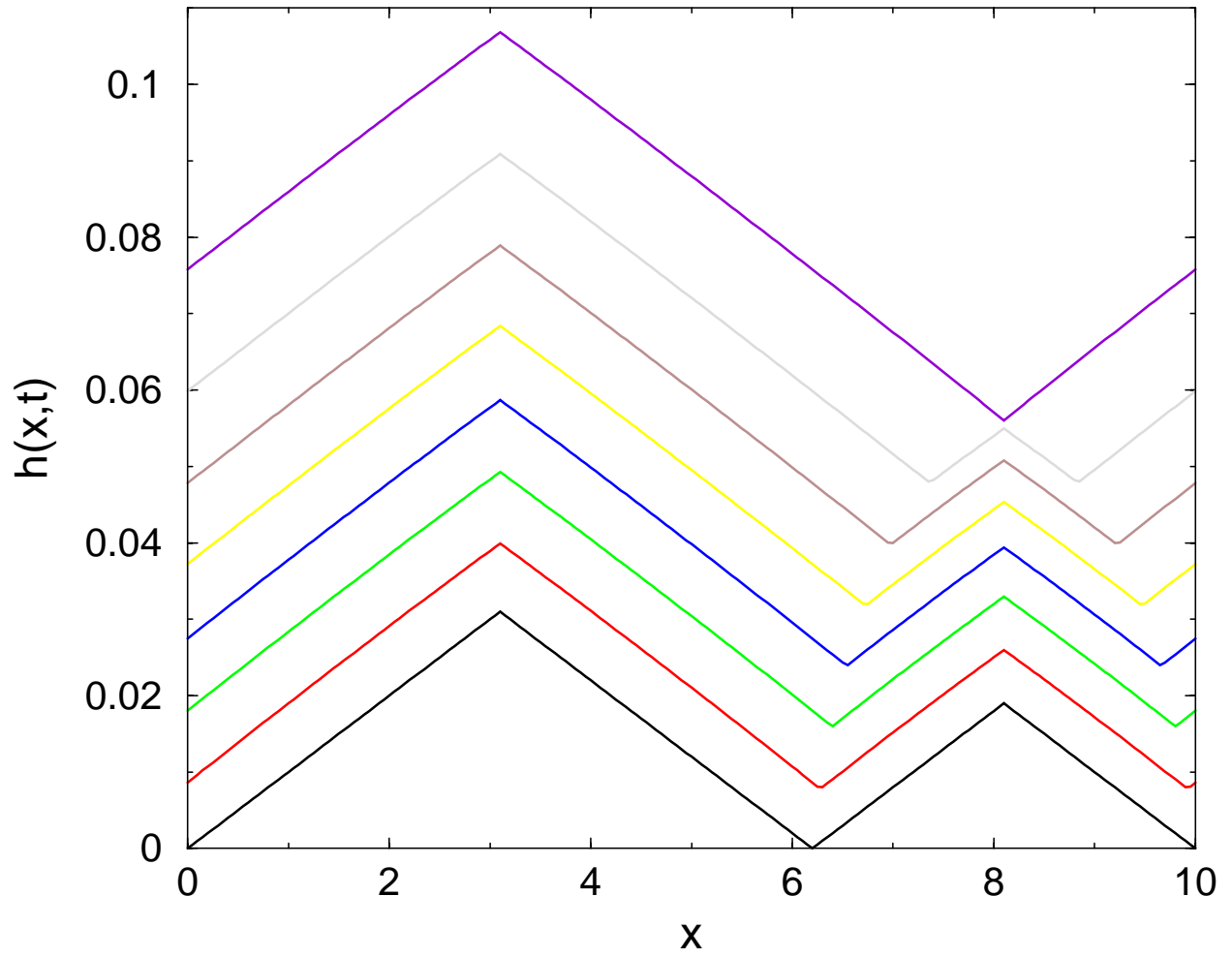


Fig. 12

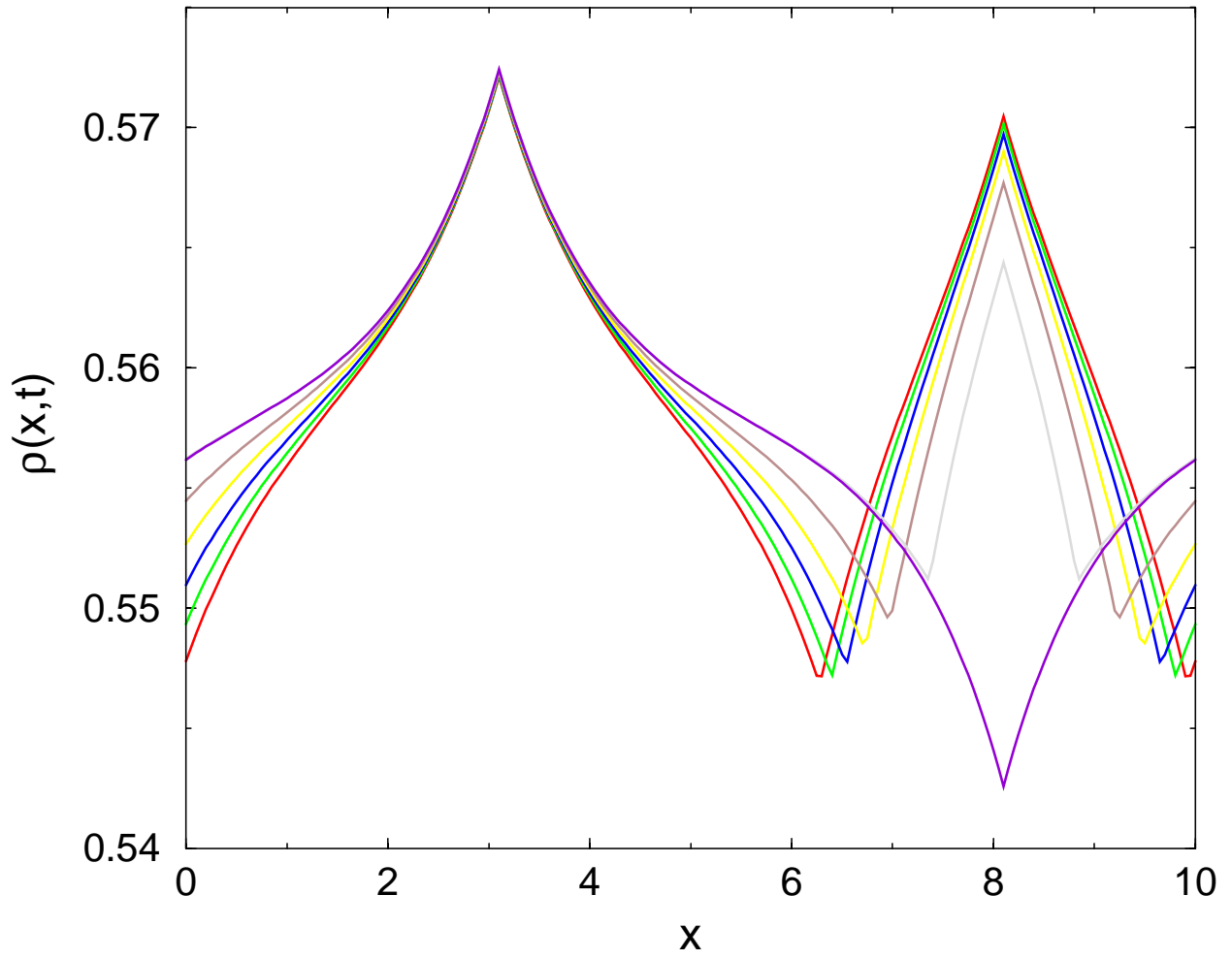


Fig. 13

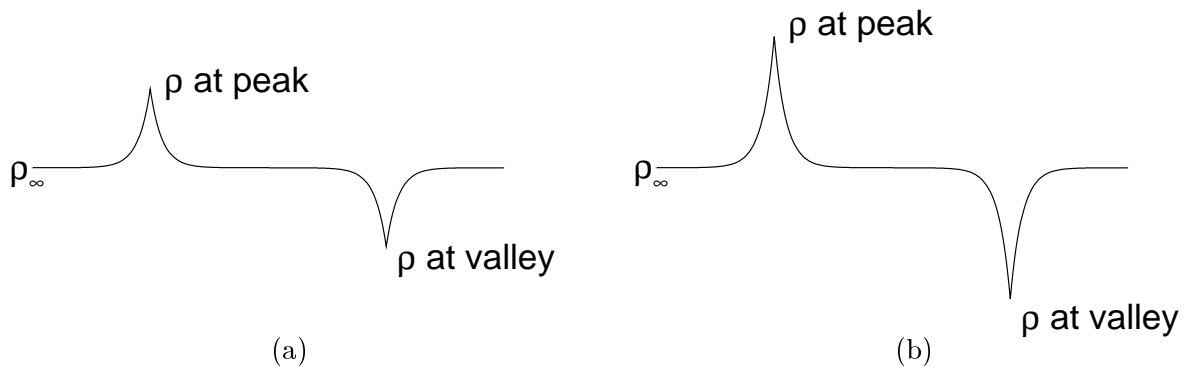


Fig. 14